Acceleration of Abramov Glacier (Pamir-Alay) retreat since the Little Ice Age

Tomas Saks, V.R. Rinterknecht, Ivan Lavrentiev, Gabriel Béra, Enrico Mattea, Martin Hoelzle

BOREAS An international journal of Quaternary research

Acceleration of Abramov Glacier (Pamir-Alay) retreat since the Little Ice Age

TOMAS SAKS, VINCENT RINTERKNECHT, IVAN LAVRENTIEV, GABRIEL BÉRA, ENRICO MATTEA AND MARTIN HOELZLE

BOREAS

Saks, T., Rinterknecht, V., Lavrentiev, I., Béra, G., Mattea, E. & Hoelzle, M. 2024 (July): Acceleration of Abramov Glacier (Pamir-Alay) retreat since the Little Ice Age. *Boreas*, Vol. 53, pp. 415–429. https://doi.org/10.1111/bor.12659. ISSN 0300-9483.

The Koksu River valley is located in the Pamir-Alay mountain range and contains 25 glaciers larger than 1 km^2 and numerous smaller glaciers. The largest glacier in the catchment is Abramov Glacier with a current surface area of 22.55 km^2 (in 2022), which was extensively monitored between 1965 and 1999, and resumed in 2011. The long and detailed mass balance time series provide, among other information, benchmark climate variables for the Pamir-Alay range. We report 10 new cosmogenic ^{10}Be exposure dates of glacial moraines directly deposited by Abramov Glacier to extend the glacial history of the valley. Six boulders indicate that the Local Last Glacial Maximum occurred at 17.1±1.0 ka. Four boulders suggest a Little Ice Age (LIA) glacial advance around AD 1750. Secular glacier mass balance reconstructions suggest a progressively negative mass balance since the LIA advance. The decrease in mass balance accelerated in the last quarter of the 20th century. Results from repeated ground penetrating radar (GPR) measurements suggest that Abramov Glacier lost about 403 million m^3 of ice volume between 1986 and 2018. Based on the reconstruction of the glacier surface, the corresponding equilibrium line altitude, which is closely correlated with the mass balance, increased by about 70 to 80 m during this period. Our results also suggest that Abramov Glacier has become increasingly out of equilibrium with the climate over the last two decades. This is supported by repeated GPR measurements of the tongue area, which indicate a dramatic decrease in glacier area and ice volume over the period 1986–2018.

Tomas Saks (tomas.saks@unifr.ch), Enrico Mattea and Martin Hoelzle, Department of Geosciences, University of Fribourg, Chemin Du Musee 4, Fribourg 1700, Switzerland; Vincent Rinterknecht, CEREGE, CEDEX 04, 13545 Aix-en-Provence, France; Ivan Lavrentiev, Institute of Geography, Russian Academy of Sciences, Staromonetnyy Pereulok 29, 119017 Moscow, Russia; Gabriel Béra, Laboratoire de Géographie Physique Environnements Quaternaires et Actuels Ringgold Standard Institution, Université Paris 1 Panthéon-Sorbonne – Géographie, 2 rue Henri Dunant, Thiais 94320, France and CEREGE, CEDEX 04, 13545 Aix-en-Provence, France; *received 5th February 2024, accepted 23rd April 2024.*

Mountain glaciers are currently in a state of global decline (Zemp *et al*. 2019), and central Asia is home to two important mountain systems – the Tien Shan and the Pamir. While the Tien Shan contains nearly 15 000 glaciers covering an area of approximately 12 300 km^2 (RGI Consortium 2017), the Pamir contains over 13 000 glaciers covering an area of approximately 12 000 km^2 (Mölg *et al*. 2018). The Pamir-Alay is composed of the Alay and Turkestan Ranges and forms the northern mountain ranges of the Pamir system. In the Pamir-Alay, mean glacier elevation follows a gradient from west (3800 m a.s.l.) to east (>5000 m a.s.l.).

Research on past glaciations in central Asia began at the beginning of the last century. The first descriptions of glacial deposits in the Pamir and Alay ranges were made by German and Austrian expeditions (Noeth 1931; Ficker 1933; Klebelsberg 1934). However, their chronological interpretations were based on Alpine Pleistocene analogues. Later work by Sidorov (1960, 1979) reported moraine evidence for two Pleistocene glaciations of decreasing extent, but these studies lack age estimates.

Bondarev *et al*. (1997) compiled and reviewed the available data on glacier fluctuations in the Caucasus, Pamir-Alay, and Tien Shan. Based on his work, it was generally accepted that four glacial stages occurred in the Pamir-Alay range. The oldest and second oldest moraine generations (Q1 and Q2) were described in the eastern and western Pamir and were interpreted to be of Early Pleistocene (1.5 and 1.0 Ma) and Middle Pleistocene (300–120 ka) age, respectively. The third moraine generation (Q3), with moraines rising to 200 m above the valley floor, was interpreted as Late Pleistocene (44–30 ka). Finally, all Holocene moraines were grouped into a fourth complex (Q4). However, this chronology was based on only a few radiocarbon dates from soils and was mostly constructed through correlations with a broader Russian continental chronology. The result is that the current state of knowledge of glacial history does not provide enough detail to detect any in-phase or out-of-phase behaviour between glaciations for the central Asian mountains and surrounding mountain ranges (Abramowski *et al*. 2006).

Over the past two decades, as cosmogenic nuclide dating has become more widely available, several studies have been conducted in the Tien Shan and Pamir. Blomdin *et al*. (2016) evaluated all available cosmogenic ages for the Tien Shan and concluded that only Marine Isotope Stage 2 (MIS 2; 15–28 ka) could be confidently defined, with glacial extent largely confined to the valleys. They also found that an unusual 60% of the ages are likely to be dominated by geological processes such as inheritance or post-depositional shielding. To date, older

DOI 10.1111/bor.12659

glacier advances in the Tien Shan have only been tentatively described. A robust MIS 3 glacial boundary can be found in the eastern sector of the Tien Shan, while MIS 5 glaciation is speculative, and there is no robustly dated evidence for glaciations during MIS 4 or 6 in the Tien Shan. In the Pamir, glaciations during MIS 1, 2, 4, 5, 7 and 9 have been identified (Zech *et al*. 2005a; Rodriguez *et al*. 2006; Seong *et al*. 2009; Röhringer *et al*. 2012; Stübner *et al*. 2021).

Little Ice Age (LIA) cosmogenic exposure dating in the Kyrgyz Tien Shan is limited to two ages reported from the Ala-Archa catchment, northern Tien Shan, of 0.343±0.088 and 0.710±0.120 ka (Koppes *et al*. 2008). Zhang *et al*. (2016) obtained several boulder exposure ages in the Nalati area, suggesting an LIA advance between 0.290±0.170 and 0.270±0.200 ka ago. Li *et al*. (2016) reported 31 ^{10}Be exposure ages in the eastern Tien Shan, suggesting a major LIA advance before about 0.430±0.100 ka ago, as well as a second advance 0.270±0.055 ka ago.

In the Pamir-Alay, surface exposure ages of glacier landforms have been determined by Abramowski *et al*. (2006), Grin *et al*. (2016), Seong *et al*. (2009), Stübner *et al*. (2021), Zech *et al*. (2005a, b, 2013). Overall, three major glacier advances were proposed during MIS 2, 4 and 5. During MIS 5 and 4, the glaciers expanded into the wide Alay valley as piedmont glaciers, whereas during MIS 2 the glaciers were confined to their valleys.

Glaciers are sensitive to their surrounding climate, and the equilibrium line altitude (ELA) at the surface of a glacier corresponds to a theoretical line that represents the lowest boundary of climatic glaciation (Ohmura 2018). Based on the mapping and dating of glacial deposits at 11 sites in five mountain ranges of central Asia, Batbaatar *et al*. (2020) showed that glaciers in humid regions advanced to their maximum extent during MIS 3–2, with ΔELA (change relative to present) ranging between 1100 and 600 m. In contrast, glaciers in the arid interior of central Asia, in the rain shadow of the Karakorum and Pamir ranges, and in the Gobi Desert ranges reached their maximum extent between MIS 6 and 4, and glacier extent during the subsequent colder/drier MIS 3–2 was significantly smaller or did not extend beyond their cirques (Batbaatar *et al*. 2020).

In this study, we present results of cosmogenic ^{10}Be exposure dating of glacial moraines in the vicinity of Abramov Glacier, central Asia. Based on our results, we reconstruct the change in glacier mass balance since the LIA and further develop the Late Pleistocene glacial history of Abramov Glacier.

Study area and previous research

Abramov Glacier is located in the Koksu River valley in the Pamir-Alay mountain range (Fig. 1). The valley is home to 25 glaciers larger than 1 km^2 and numerous smaller glaciers (according to RGI Consortium 2017). Abramov Glacier was the focus of continuous glacier mass balance monitoring and other scientific studies between 1967 and 1999 (Glazirin 1993). Monitoring efforts have recently been resumed (Hoelzle *et al*. 2017). The long and detailed mass balance time series provide benchmark climate variables for the Pamir-Alay range and beyond (Barandun *et al*. 2015, 2020; Hoelzle *et al*. 2017; Kronenberg *et al*. 2022).

The first reconstruction of palaeo-glacial advance and geomorphological map for the Koksu valley were provided by Suslov (1972). He interpreted the most extensive glaciation to have occurred during the middle Quaternary (Matchinski stage), when Abramov Glacier reached the lower part of the Koksu valley (2500 m a.s.l.) (Fig. 1). However, his interpretation is mainly based on correlation with the glacial chronology established for Siberia (Bondarev *et al*. 1997).

Zech *et al*. (2000) attributed the moraine at 2500 m a.s.l. to the LGM advance (Fig. 1). However, these hypotheses were challenged by Abramowski *et al*. (2006). They suggested a much older moraine deposition during the late Quaternary (62–72 ka), based on ^{10}Be exposure dating of boulders from the top of a lateral moraine located on the right bank of the Koksu River close to its tributary at an elevation of approximately 2500 m a.s.l. (Fig. 1). Since then, the ice has retreated some 45 km upvalley, where boulders from a moraine dated to about 14 ka are found 3100 m a.s.l. (Abramowski *et al*. 2006).

Zech *et al*. (2000) carried out geomorphological mapping and ^{14}C dating of palaeosols in the valley. They identified several moraines in the valley at 3100, 3200, 3300 and 3350 m a.s.l. (Fig. 2), approximately 10 km from the modern snout of Abramov Glacier. We recently visited these moraines during a fieldwork campaign and suggest a reinterpretation of the moraine at 3100 m a.s.l. as a glaciotectonic ridge with a core of solid bedrock rather than a frontal moraine. Further upvalley, a moraine at 3440 m a.s.l. was suggested to have been deposited during the Early Holocene or possibly during the Lateglacial. Poorly preserved remnants of a moraine 1.5 km downvalley from Abramov Glacier snout were found at 3550 m a.s.l. Zech *et al*. (2000) interpreted the time of deposition of this moraine to correlate with a Neoglacial glacier advance and they calculated an ELA decrease of 50 m relative to the present. Finally, relics of a moraine at 3560 m a.s.l. were interpreted to represent the maximum glacier advance during the LIA. Currently, Abramov Glacier terminates at approximately 3650 m a.s.l.

Using the growth of *Aspicilia* lichens, Solomina & Kamnyanskiy (1998) established a chronology for Abramov Glacier fluctuations during the Late Holocene. Major ice advances were identified in the 15th century and at the end of the 16th, 18th, and 19th centuries. During the 20th century, Abramov Glacier expanded until 1912, before a pronounced retreat began in 1928.

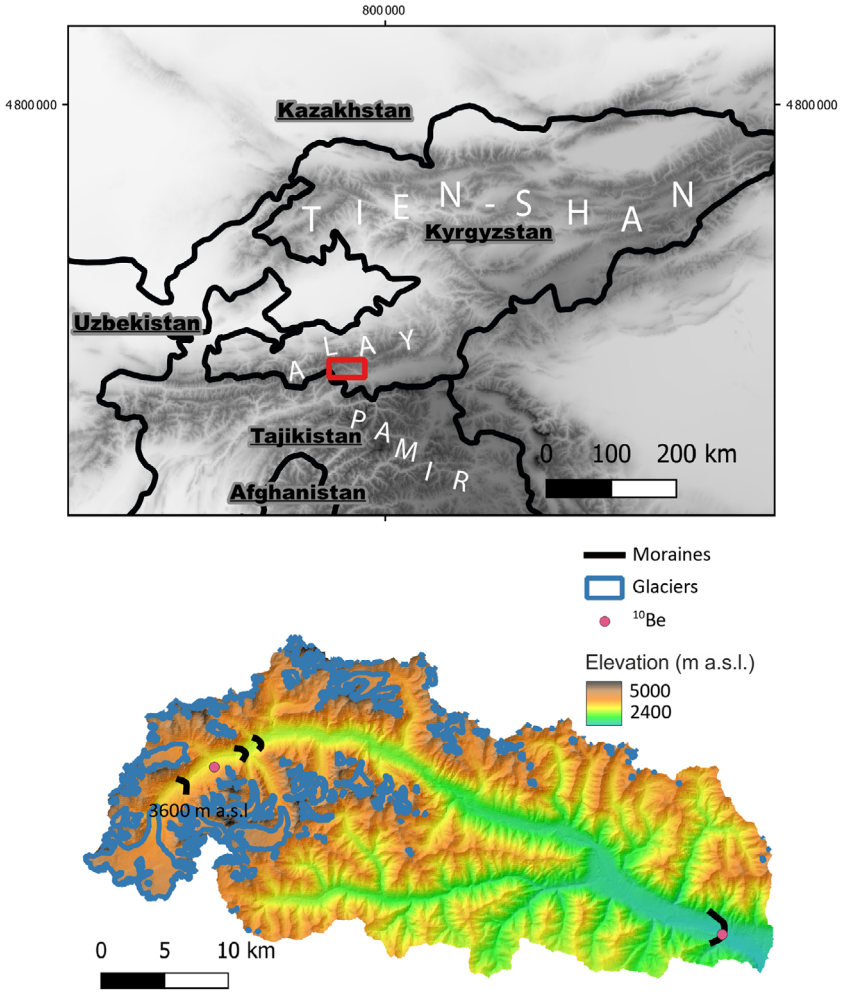

Fig. 1. Location of the study area. Red box depicts the Koksu river catchment, while glaciers are shown in blue. ^{10}Be sites are from Abramowski *et al.* (2006).

The last glacier advance was recorded in 1972/73 when Abramov Glacier advanced by approximately 400 m (Glazirin 1993).

Based on geomorphological mapping Glazirin (1993) reconstructed the marginal positions of Abramov Glacier (Fig. 2) and suggested that the glacier tongue was at approximately 3560 m a.s.l. in 1850. Mandychev *et al.* (2017) used these outlines to reconstruct the glacier retreat, though they assumed the same age as Glazirin (1993) for the LIA Abramov Glacier extent.

First ice thickness measurements on Abramov Glacier were performed in 1970–72 with 440 MHz radio altimeters RV-2 and RV-17 at 300 points along 12 profiles (Ryumin 1972) but the network of measuring points was not enough to construct comprehensive ice thickness and bedrock elevation maps. In 1986 a complete ground-based radar survey with low-frequency mono-pulse radar MPI-8 (central frequency 8 MHz) allowed for the construction of complete ice thickness distribution and bedrock topography maps of this glacier (Vasilenko *et al.* 1988; Kuzmichenok 1990). Point ice thickness measurements were performed during 3 weeks from 26th June to 14th July 1986 along with geodetic referencing of each of 682 points distributed over the glacier surface every 100–200 m. The common mid-point (CMP) method was used for radio wave velocity (RWV) measurements at two points on the terminus and the accumulation area provided close values of RWV in glacier – 160.6 and 161.3 m ns^{-1}. The mean value 161 mns^{-1} then was used for time to depth conversion and construction of ice thickness distribution map. The maximum ice thickness measured was 246 m in the accumulation area and up to 220 m in the ablation area.

Material and methods

^{10}Be surface exposure dating

For ^{10}Be surface exposure dating, pieces of rock of up to 2 cm thick were loosened by a hammer and chisel from

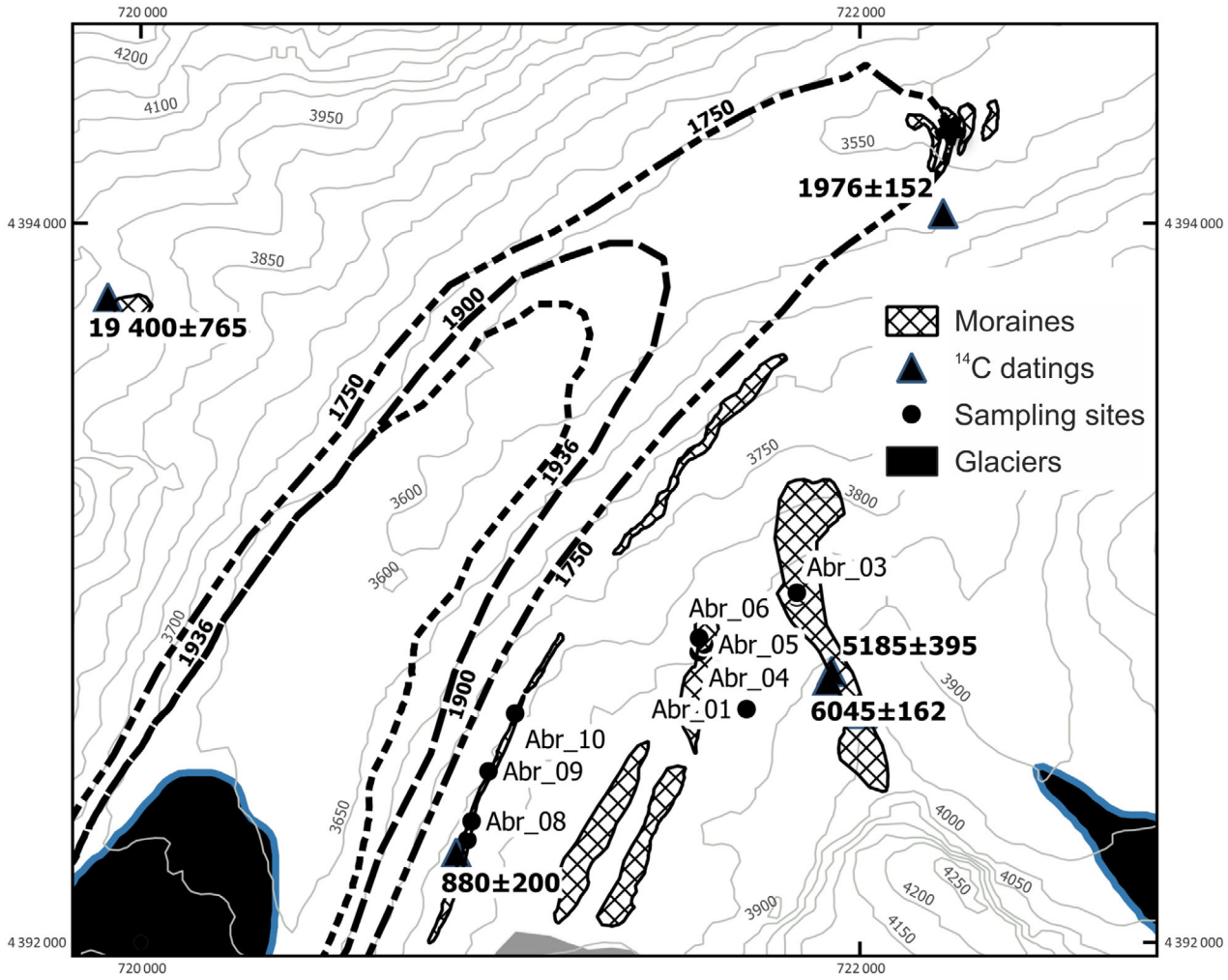

Fig. 2. Schematic map of the sampling sites and the geomorphological setting of the study area. Circles denote the locations of the cosmogenic ^{10}Be samples of this study with their corresponding sample number. Triangles denote palaeosol sampling sites with the corresponding ^{14}C ages reported in Zech *et al.* (2000). The radiocarbon ages were recalculated using the software Calib8.2 and the calibration curve IntCal20 (Reimer *et al.* 2020). Dashed lines depict Abramov Glacier positions according to Glazirin (1993) and Mandychev *et al.* (2017). Note that in Glazirin (1993) and Mandychev *et al.* (2017), the Abramov Glacier extent of 1750 is interpreted as the limit of 1850. The star denotes the lichenometry dating site of Solomina & Kamnyanskiy (1998).

the top central surfaces of the largest boulders positioned at the top of selected moraines. We sampled 10 boulders, six on the moraine complex further from the glacier and four from the lateral moraine closer to the glacier valley (Fig. 2). All samples were collected from granite/granodiorite boulders (Table 1) with the aim of obtaining the minimum deposition age of these moraines. Boulders showing signs of spalling or recent dislocation were avoided. Positions and altitudes were recorded with a hand-held global positioning system (GPS) receiver. Topographic shielding and surface inclination of the boulder surfaces were recorded using a compass and clinometer.

^{10}Be sample preparation and analysis

Quartz bearing lithologies are suitable for ^{10}Be dating and the quartz content of the samples ranges between 10 and 80%. Samples were prepared at the CALM (Cosmonucléides Au Laboratoire de Meudon) laboratory in France. All samples were crushed and sieved in order to isolate the 250–710 µm fraction. We used magnetic separation and mineral froth flotation techniques (Herber 1969; Nichols 2019) prior to chemical etching procedures modified from Kohl & Nishiizumi (1992) to separate and purify the quartz fraction. Quartz purity was assayed using ICP-OES analysis with aluminium concentration ranging between 2 and 219 ppm.

Up to 460 µL of a commercial ^{10}Be carrier (Scharlau 998±4 mg L^{-1}) was added to each sample. Beryllium extraction was carried out using a method modified from Child *et al.* (2000). Beryllium isotope ratios in the samples and one procedural blank were measured at ASTER, the French Accelerator Mass Spectrometer

Table 1. Sample characteristics and dating results.

Sample ID	Latitude[1] (DD)	Longitude[1] (DD)	Elevation (m a.s.l.)	Thickness (cm)	Shielding[2]	Quartz (g)
ABR-01	39.6549	71.5839	3865	0.3	0.975	20.50
ABR-02	39.6577	71.5857	3888	1.1	0.982	15.70
ABR-03[6]	39.6578	71.5857	3890	0.8	0.991	23.20
ABR-04	39.6564	71.5825	3859	0.5	0.979	13.20
ABR-05	39.6566	71.5827	3845	1.6	0.979	24.72
ABR-06	39.6568	71.5825	3845	2.0	0.984	25.50
ABR-07[6]	39.6518	71.5748	3797	0.9	0.993	17.70
ABR-08	39.6523	71.5749	3787	1.1	0.988	17.30
ABR-09	39.6535	71.5756	3793	1.7	0.988	26.30
ABR-10	39.6550	71.5765	3796	1.3	0.986	22.90
	[^{10}Be][3] (10^4 at g^{-1})	Exposure age[4] (^{10}Be ka)				
Lateglacial moraine[5] 17.1±1.0 (0.5) ka						
ABR-01	96.20±2.27	17.8±0.4				
ABR-02	91.35±2.45	16.7±0.5				
ABR-03[6]	62.41±2.01	11.8±0.4				
ABR-04	84.03±2.67	15.6±0.5				
ABR-05	100.20±2.70	18.7±0.5				
ABR-06	89.11±1.84	16.8±0.3				
LIA moraine[5] 271±74 (68) ka (1747 CE)						
ABR-07[6]	5.78±0.68	1.2±0.1				
ABR-08	1.60±0.63	0.4±0.2				
ABR-09	0.93±0.42	0.2±0.1				
ABR-10	1.08±0.42	0.2±0.1				

Samples were taken from granitic and pegmatic boulder tops:
[1]With reference to WGS84 datum.
[2]Calculated using the CRONUS-Earth shielding calculator, wrapper script 1.1, main calculation 1.1.
[3]All samples were processed at the CALM (Cosmonucléides Au Laboratoire de Meudon) laboratory, France. All samples were measured at the ASTER facility using the STD11 ^{10}Be standardization.
[4]All ages calculated using the online exposure age calculator formerly known as the CRONUS-Earth online exposure age calculator version 3 (http://hess.ess.washington.edu/math/v3/v3_age_in.html; Balco *et al.* 2008) with a time-dependent production rate model and according to the Lal (1991)/Stone (2000) scaling scheme (Lm). A standard atmosphere and an estimated rock density of 2.7 g cm^{-3} were used. No erosion was accounted for. Analytical uncertainties (reported as 1σ) include a conservative 0.5% uncertainty based on long-term measurements of standards, a 1σ statistical error on counted ^{10}Be events, and the uncertainty associated with the chemical and analytical blank correction, which yielded a ^{10}Be/^{9}Be ratio of 6.12×10^{-15}.
[5]Based on the exposure age average, with no correction for erosion or snow cover (see text for discussion). Errors are reported at 1σ and include uncertainties in the Lm cosmonuclide production scaling scheme, the analytical uncertainties, as well as the uncertainties associated with the reference production rate. These ages are discussed in the text. Errors in parentheses correspond to the analytical error only.
[6]Sample excluded from the moraine age based on Chauvenet's criterion (see text for discussion).

located at CEREGE, Aix-en-Provence (Arnold *et al.* 2010). Data were normalized directly against an in-house standard STD-11 with an assigned ^{10}Be/^{9}Be ratio of $(1.191 \pm 0.013) \times 10^{-11}$ (Braucher *et al.* 2015) and a ^{10}Be half-life of $(1.387 \pm 0.012) \times 10^{6}$ years (Chmeleff *et al.* 2010; Korschinek *et al.* 2010).

Analytical uncertainties (reported as one sigma) include a conservative 0.5% uncertainty based on long-term measurements of standards, a one sigma statistical error on counted ^{10}Be events, and the uncertainties associated with the chemical and analytical blank correction: the ^{10}Be/^{9}Be blank ratio was 6.12×10^{-15}.

^{10}Be surface exposure age calculation

To determine surface exposure ages from the ^{10}Be concentrations measured in the quartz fractions, we used a modern global ^{10}Be production rate at sea level and high latitude derived from the primary calibration data set of Borchers *et al.* (2016), and the online exposure age calculator version 3 of the online exposure age calculator formerly known as CRONUS-Earth (Balco *et al.* 2008). We report here the exposure ages calculated with the 'Lm' scaling schemes (Table 1). The 'Lm' method provides the closest fit to existing calibration data and uses the scaling factors proposed by Lal (1991) and Stone (2000) and can be further accommodated for palaeomagnetic corrections following the description of Nishiizumi (1989). As such, we think that the exposure ages calculated with this scaling method (Lm) represent the best age estimations of the exposure of the samples. Using the Lifton–Sato–Dunai (LSD) scaling scheme by Lifton *et al.* (2014) would increase our exposure ages younger than 1000 years by up to 7% and decrease our exposure ages older than 15 ka by as much as 6%. The online calculator makes sample-specific corrections for thickness and density (we assumed a density of 2.7 g cm^{-3}). The production rates could be further affected by intermittent snow cover, vegetation cover,

and erosion rate. We do not apply any correction for these factors. Snow is not anticipated to have accumulated for long periods of time on high boulders or high grounds, prone to high winds. Vegetation is mostly composed of mosses and lichens as samples were taken above the tree line. Evidence of glacial polish has been recorded on several boulder surfaces and is evidence of low post-glacial erosion rate. We corrected the surface production rates for topographic shielding due to surrounding topography using the online topographic shielding calculator available at: http://hess.ess.washington.edu/math/ (accessed 20.04.2022). In addition, the surface production rate for sample ABR-07 was corrected for a surface slope dipping by 10 degrees.

Secular mass balance estimation

Secular glacier mass balance is a simple, yet robust tool to estimate the regional climate change effects on mountain glaciers (Haeberli & Hoelzle 1995). Secular glacier mass balance calculation is based on an approach that considers the step changes after the full dynamic response and once a new equilibrium of the glacier has been achieved (Haeberli & Hoelzle 1995; Hoelzle *et al.* 2003, 2007). This equilibrium is achieved when mass balance disturbance Δb leads to a corresponding glacier length change ΔL that depends on the original length L_0 and the average annual mass balance (ablation) at the glacier terminus b_t:

$$\Delta b = b_t \times \Delta L_0 \quad (1)$$

The dynamic response time t_{resp} is calculated following Johannesson *et al.* (1989), where h_{max} is the ice thickness, usually taken at the equilibrium line where ice depths are near maximum.

$$t_{resp} = h_{max}/b_t \quad (2)$$

Assuming a linear change of the mass balance from b to zero during the dynamic response, the mean specific mass balance $<b>$ can be calculated according to Equation 3. $<b>$ values are annual ice thickness change (metres of water equivalent (we) per year) averaged over the entire glacier surface, which can be directly compared with values measured in the field. Although the method is quite simple, the results compare very well with long-term observations (Hoelzle *et al.* 2003). The factor n_{resp} denotes the count of possible response times within the considered time period, which cannot be larger than the calculated response time by Equation 2 for each glacier. In this study, for the mass balance reconstruction, we relied primarily on the known glacier length change observations close to the calculated response time.

$$< b > = \Delta b/2\, n_{resp} \quad (3)$$

Ground penetrating radar (GPR) measurements

The most recent measurements of ice thickness were conducted in January 2018 during a field campaign organized by the University of Fribourg, Switzerland. The ground-based survey was performed on Abramov Glacier with a 20 MHz VIRL-7 monopulse radar (Vasilenko 2011; Fig. 3). Measurements (profiling) were carried out automatically at a frequency of 0.4 s. Radar components (transmitter, receiver, control unit, batteries, and GPS) and antennas were mounted on two plastic sledges towed by one operator on skis along 24.6 km of profiles (Fig. 4). A conventional GPS was used to record plane coordinates every 2 s. For the transmitting and receiving of radar signals, resistively loaded dipole antennas of 5.8 m long were used, with a distance between their centres of 10 m. To synchronize the signals from antennas, a fibre optic cable was used. The mean distance between measurement points varied from 0.2 to 0.4 m.

For visualization and further processing of GPR data the RadExPro Plus 2011.1 software (www.radexpro.ru; Kulnitsky 2000) was used. Standard procedures of amplitude correction, bandpass filtering, 2D spatial filtering and Stolt-FK migration (to obtain the real geometry of the bedrock by correcting the position of the lateral reflections using Fourier analysis) were applied to the raw radar data (Fig. 3). Picking was used for manual digitizing of the time delay of reflected signals in interactive mode.

After data processing a summary table of UTM coordinates (x, y) and the delay time (τ) of the digitized bedrock was compiled and the glacier thickness was calculated using a constant speed of 0.161 mns^{-1} for radio wave propagation in the glacier (Dowdeswell 2004). In the final step, ice thickness point data, together with data on zero thickness at glacier margins were used to construct the ice thickness maps using the Topo-to-Raster interpolation method in ArcGIS 10.6 software. The accuracy of bedrock reflection determination (and further ice thickness data) was estimated by data comparison at the 27 profile intersections and amounted to ±1%.

Glacier reconstruction

Based on reconstructed Abramov Glacier outlines (Mandychev *et al.* 2017) and bed elevation obtained from GPR investigations (Kuzmichenok 1990), theoretical ice surface profiles were reconstructed for the LIA glacial stage. Resultant ice surface profiles were used to produce a LIA ice surface DEM of Abramov Glacier using the Profiler v.2 spreadsheet (Benn & Hulton 2010) and extended with the GlaRE tool (Pellitero *et al.* 2016). The ice surface profiles were used to produce an ice surface model for the Abramov Glacier LIA stage. One of the biggest sources of uncertainty for this approach is

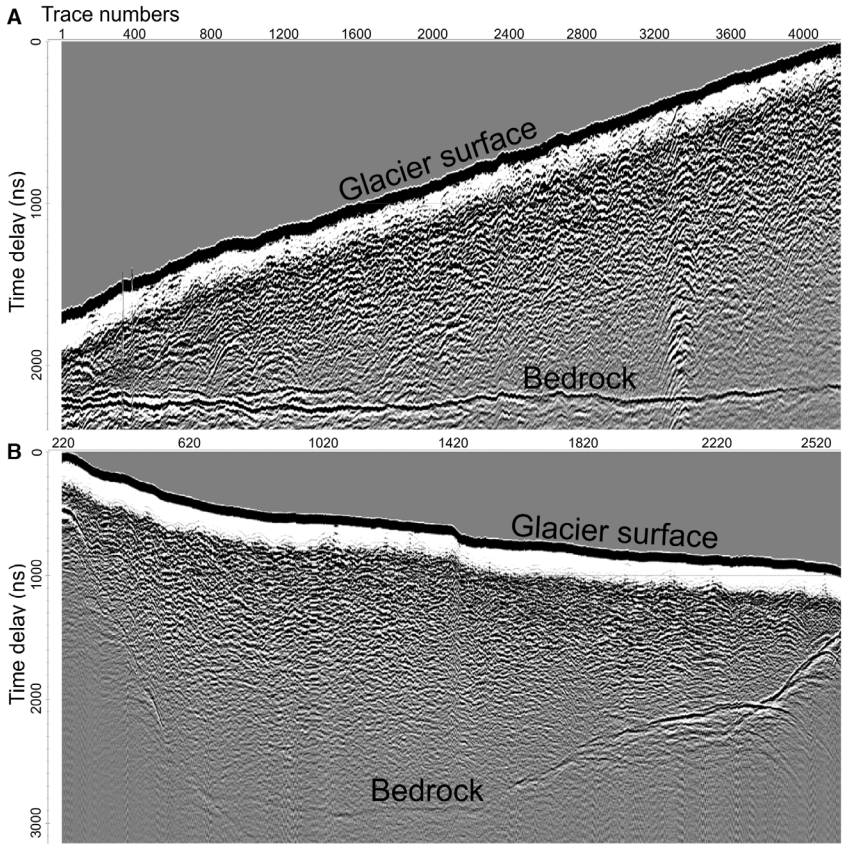

Fig. 3. Typical radargrams obtained on Abramov Glacier in 2018 with 20 MHz radar. A. Longitudinal profile 1–1′. B. Transversal profile 2–2′. Location of profiles is shown in Fig. 4.

the lack of information about the basal shear stress. Abramov Glacier thickness distribution and bed topography were mapped in 1986 by Kuzmichenok (1990). We used these data to tune shear stress values in places of known thickness. For the LIA glacial stage reconstruction, we further used the obtained basal shear stress values, while for the extended tongue area basal shear stress values were extrapolated.

The ELA of the LIA glacial stage was determined from the reconstructed glacier hypsometry through the area–altitude ratio (AAR) and the area–altitude balance ratio (AABR) methods by applying the GlaRe tool (Osmaston 2005; Pellitero *et al.* 2016). Both methods rely heavily on the accuracy of the reconstructed glacier hypsometry, which, in turn relies on assumed basal shear stress values, yet glacier slip remains poorly understood. Moreover, glacier dynamics might change in time by evolving of glacier bed (Brædstrup *et al.* 2016).

To reconstruct Abramov Glacier geometry during the LIA we used a highly modified version of the glacier flow model (GFM) developed by Unterfinger & Luck (2023). The model simulates glacier flow on a DEM grid, by combining the shallow-ice approximation (Fowler & Larson 1978) with the *fracd8* flow routing method, adapted from the D8 algorithm (O'Callaghan & Mark 1984). Mass balance for each grid cell is calculated from the DEM altitude: compared to the original model, we introduced the use of two different vertical gradients above and below the ELA, as well as a feedback effect between ice thickness, surface elevation and mass balance. We also implemented empirical topographic controls on mass balance according to surface slope, aspect, and curvature: these mimic the effects of avalanches, differential melt rates driven by solar radiation, preferential snow deposition and wind erosion (Evans & Cox 2005; Huss *et al.* 2021). Moreover, we adapted the *fracd8* routing algorithm used in the model, in order to use multiple sub-annual timesteps: this change accommodates annual ice displacements larger than the grid cell size. We additionally included a minimum parametrization of basal sliding velocities (Weertman 1964):

$$\tau_b{}^m = \rho_{ice} \times g \times h \times \tan \alpha \quad (4)$$

$$u_b = C \times \tau_b{}^m \quad (5)$$

where $\tau_b{}^m$ is basal shear stress, ρ_{ice} is ice density, g is gravity, h is ice thickness, α is surface slope, u_b is basal

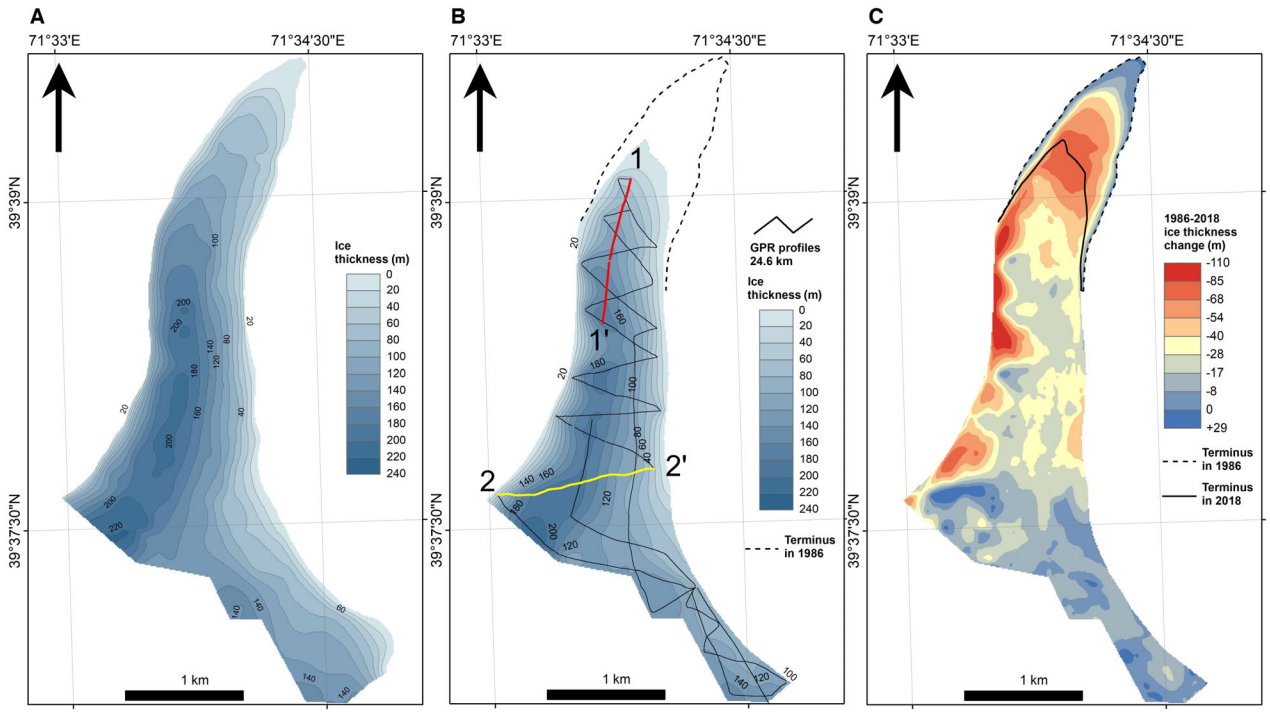

Fig. 4. Ice thickness distribution of the lower part of Abramov Glacier in 1986 (after Vasilenko *et al.* 1988) (A), in 2018 with scheme of GPR profiles (B), and ice thickness change from 1986 to 2018 (C).

sliding velocity and we set $C = 1$, $m = 1/3$. Finally, following Cuffey & Paterson (2010) we adapted the computation of ice flow between cells as:

$$u_d = 0.9\, u_s \quad (6)$$

where u_d and u_s are respectively depth-averaged and surface ice velocities.

For simulation purposes we used Copernicus DEM (https://doi.org/10.5270/ESA-c5d3d65) with a grid size of 25 m while the glacier bed was obtained from the GPR investigations by Kuzmichenok (1990). Other glacier bed elevations were obtained by subtracting available modelled glacier thickness data from Farinotti *et al.* (2019). For the simulations, we used the mass balance gradient of 0.0076 m w.e. m^{-1} for the ablation area (according to Barandun *et al.* (2015) and Kronenberg *et al.* (2021)) and 0.0022 m w.e. m^{-1} for the accumulation area (Barandun *et al.* 2015; Gastaldello 2022). For calculation of the ELA for the LIA stage, several cooling scenarios were run until the new glacier position matched the observed extent in the field.

Results

^{10}Be exposure dating

Six exposure ages from the moraine furthest away from the glacier range between 11.8 and 18.7 ka. Four exposure ages from the moraine closest to the glacier terminus range between 0.2 and 1.2 ka. We tested each moraine population for statistical outliers using Chauvenet's criterion (Taylor 1997), a criterion identifying samples that have <50% probability of falling within the normal distribution of the sample population. Samples ABR-03 and ABR-07 were identified as outliers and were removed from the sample populations before calculating the moraine ages. For each moraine, we report the average time of deposition and their associated uncertainties, which include the analytical uncertainties and the uncertainties associated with the production rate (Table 1).

Surface exposure ages form two clusters with mean minimal ages of 17.1±1.0 and 0.271±0.074 ka.

Ground penetrating radar results

The GPR results suggest depletion of the ice in the glacier tongue area (Fig. 4). In total, from 1986 to 2018 Abramov Glacier lost approximately 0.56 km^2 in ice-covered area and 403 million m^3 in ice volume (Table 2). A typical radargram is shown in Fig. 3, which was taken along the flowline in the glacier tongue area, showing a sharp reflection of the glacier bed.

A map of ice thickness distribution was constructed for the investigated part of the glacier covering an area of 3.7 km^2. The maximum measured ice thickness reaches 219 m while the mean value is 120 m. Comparison with

Table 2. Ice thickness and ice volume of the previously measured part of Abramov Glacier and its changes from 1986 to 2018 based on GPR data.

	Ice thickness (m)			Ice volume (million m^3)	Area change (km^2)	Volume change (million m^3)
	Min.	Max.	Mean	2018	1986–2018	
Measured	12	219	120	388.21	0.56	129.96
Interpolated	0	218	103	–	–	–

previous ice thickness data obtained in 1986 according to Vasilenko *et al.* (1988; digitized map) revealed significant reduction of ice thickness and volume (Table 2, Fig. 4C). Shrinkage of the glacier length (up to 1 km) led to the disappearance of about 0.56 km^2 of ice in the terminus area, which corresponds to 21.91×10^6 m^3 of its ice and an additional 108.05×10^6 m^3 of ice caused by thinning of the studied area.

Glacier reconstruction

The present-day ELA lies approximately at 4150 m a.s.l. (Kronenberg *et al.* 2021), though the year-to-year variability is high (Fig. 5). Similarly, the AAR varies from 18 up to 82%, with a value corresponding to the balanced conditions of 65% (Fig. 5). Based on the point measurements on the glacier for the time period 2012–2020 (WGMS 2021), we calculated the AABR with a value of 2.9. We used both the AAR and AABR methods to calculate the ELA changes since the LIA by applying the GlaRe tool (Pellitero *et al.* 2016) based on the LIA glacier surface reconstruction. The AAR method yields an ELA of 4203 m a.s.l. for the current glacier setup, and 4176 m a.s.l. for the LIA stage, suggesting an approximately 30 m depression of the ELA. This result should be interpreted with caution, as during the LIA the AAR was probably lower due to a proportionally larger tongue area of Abramov Glacier. ELA calculation using the AABR method (assuming an AABR value of 2.9) yields an elevation of 4153 m a.s.l. for the current glacier extent and 4076 m a.s.l. for the LIA stage, suggesting an approximately 80 m depression of the ELA. Mass balance series suggest a similar ELA for the current glacier extent (Fig. 5), partly validating the calculated results.

To reconstruct the glacier extent and estimate the ELA during the LIA with the glacier flow model we first found the steady-state solution that reproduces the current glacier extent and thickness distribution (Fig. 6), i.e. $db/dz = 0.0076$ m w.e. m^{-1} for the ablation area, $db/dz = 0.002$ m w.e. m^{-1} for the accumulation area and an ELA at 4080 m a.s.l. The steady-state solution with

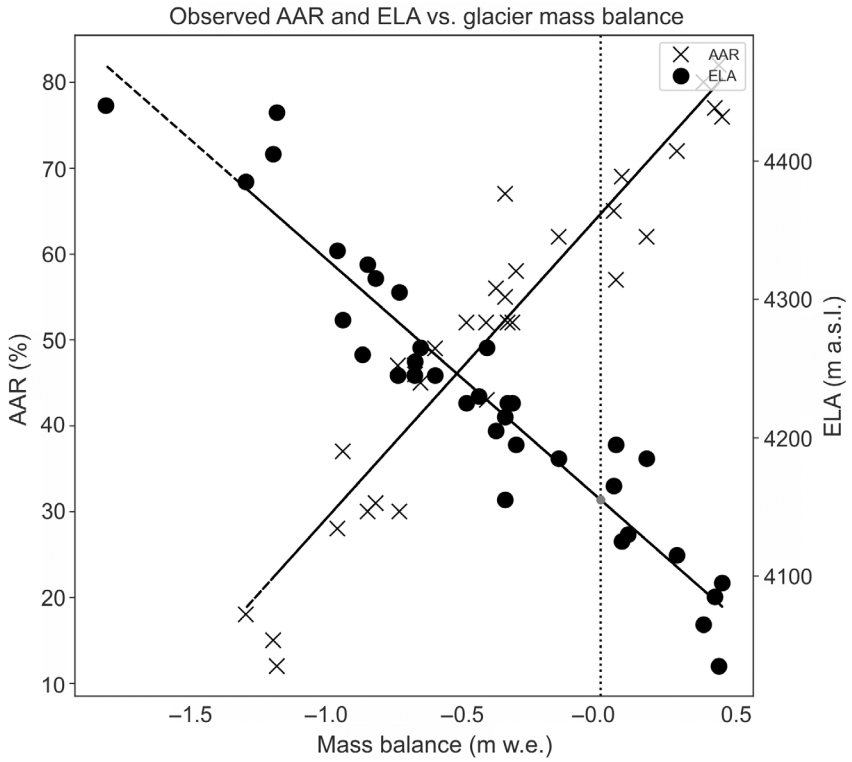

Fig. 5. Comparison of observed AAR (indicated by crosses) and ELA (indicated by dots) with glacier mass balance for the time period 1968–2016.

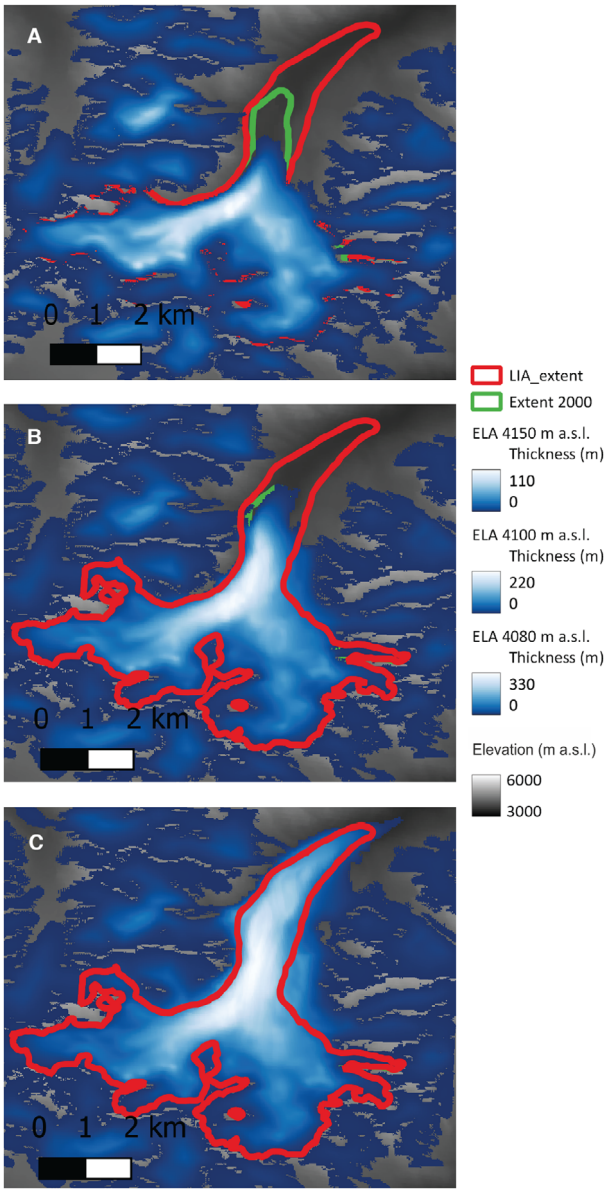

Fig. 6. Glacier flow model (GFM) simulated glacier extent for the (A) steady state solution for an ELA at 4150 m a.s.l.; (B) present-day glacier extent with an ELA at 4100 m a.s.l. (according to RGI Consortium 2017) and (C) LIA extent of Abramov Glacier. Note that other glaciers in the valley also significantly increased during the LIA glacial stage.

the current ELA of 4150 m a.s.l. yields a solution where the glacier retreats by some 1400 m, as well as loses more than half of its volume (Fig. 6A), suggesting that Abramov Glacier is in strong disequilibrium with the current climatic forcing. To simulate the current extent of Abramov Glacier, the ELA had to be lowered to 4100 m a.s.l. (Fig. 6B). As can be seen, the model thickness distribution corresponds well to the observations. The LIA extent was reached by gradually lowering the mean ELA in 10-m steps until the theoretical LIA extent was reached (Fig. 6C), resulting in a ΔELA of around 80 m as compared to the initial steady state with an ELA at 4150 m a.s.l.

The other glaciers in the modelling area display larger initial extents as well as much more pronounced glacier advances in the cooling scenario. This effect occurs because for all the glaciers only one set of initial conditions can be used, i.e. the one for Abramov Glacier, causing other glaciers to advance more strongly due to their much steeper bed geometry.

Glacier secular mass balance reconstruction

The reconstructed glacier length change allows calculation of the secular glacier mass balance since 1750 (Fig. 7). For calculation of the secular glacier mass balance, the glacier response time was determined. Ground penetrating radar measurements suggest that the current maximum thickness of Abramov Glacier is 230 m (Kronenberg *et al.* 2021). The available point stake measurements from the WGMS database (WGMS 2021) at the tongue suggest a b_t of around −4.6 to −6.3 m w.e. For the current study, a value of −6 m w.e. was chosen, yielding a response time (t_{resp}) for Abramov Glacier of approximately 38 years.

The length change measurements available in the WGMS database had to be corrected. First, the age of the glacier margin position in 1850 was changed to 1750. Secondly, the reported length change of −572 m between the glacier margin positions of 1900 and 1750 does not correspond to the actual length change, which is approximately −890 m. The source of this discrepancy is unclear. Calculated secular glacier mass balance gradually decreased from 1750 until the mid-20th century, and mass loss accelerated after the mid-20th century (Fig. 7). Considering that the average mass balance gradient for Abramov Glacier is 0.0076 m w.e. m^{-1} (Kronenberg *et al.* 2021) we suggest that the mean mass balance $<b>$ for the whole period since the LIA was around −0.32 m w.e.

Discussion

We interpret the cluster of the older exposure ages (from 15.6±0.5 to 18.7±0.5 ka) as representing the Local Last Glacial Maximum (LLGM) in the Koksu valley. This age range falls well within the generally accepted timing of the LLGM in the Pamir-Alay (Abramowski *et al.* 2006; Seong *et al.* 2009; Zech *et al.* 2013; Grin *et al.* 2016). Zech *et al.* (2000) developed a geomorphological map of the Koksu valley, identifying 10 moraines (Fig. 8). They interpreted the LLGM moraine at 2500 m a.s.l., but later exposure ages obtained by Abramowski *et al.* (2006) suggested a MIS 4 age for this moraine. We suggest that during the LLGM the glacier tongue terminated at an altitude between 3100 and 3350 m a.s.l., with a corresponding ELA lowering of 200–300 m as calculated by Zech *et al.* (2000). During this advance,

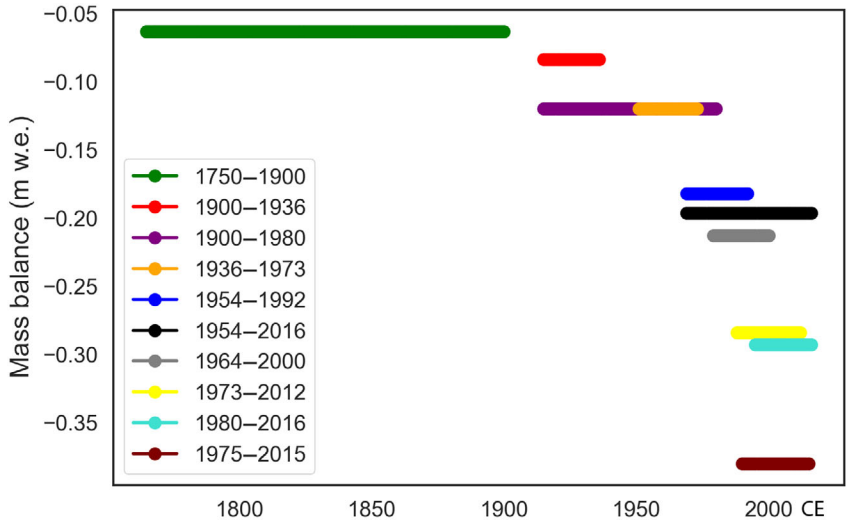

Fig. 7. Calculated mean secular mass balance <*b*> for Abramov Glacier since 1750 and comparison with the calculated geodetic mass balance for the time period 1975–2015 by Denzinger *et al.* (2021).

Abramov Glacier likely merged with adjacent glaciers in the Koksu valley, resulting in a glacier surface of roughly 133 km^2. Unfortunately, there are no exposure ages available so far for the frontal moraines in the valley, and the ages of the two moraines at 3350 and 3300 m a.s.l. remain unknown.

Zech *et al.* (2000) carried out several ^{14}C dating of palaeosols in the study area (Fig. 2). The soil sample on the western slope from the side moraine was dated to 15 950±350 a, suggesting that this area became ice-free some time before. The sampling site is some 70 m higher than the moraines we sampled on the eastern slope. The ^{14}C dating of the soil (3950 m a.s.l.) from the moraine on the orographic right side yielded an age of 24.3±1.16 ka, suggesting the maximum age of the LGM in the study area.

There are two more terminal moraines at 3200 and 3300 m a.s.l. that have currently undefined ages (Fig. 8). Abramowski *et al.* (2006) obtained exposure ages of three boulders located on what they interpreted to be a lateral moraine some 6 km down the valley from the Abramov Glacier snout with ages ranging between 13.8 and 14.1 ka. They suggested a Younger Dryas age for this moraine, even though these ages pre-date the global Younger Dryas event by some 2 ka (Cheng *et al.* 2020). We suggest that this lateral moraine is part of the LLGM moraine complex, correlating with the terminal moraines at the elevations of 3300 and 3200 m a.s.l. Additional cosmogenic ^{10}Be dating of these three moraines will validate or invalidate our hypothesis about the glacier evolution during the LLGM stage and, possibly, other glacier stages.

We interpret the cluster of younger exposure ages (from 0.2±0.1 to 0.4±0.2 ka) as representing the glacier advance during the LIA. Seong *et al.* (2009) carried out boulder exposure dating in the semiarid western-most part of Tibet, suggesting possible late ice advances at 1.4±0.1 ka and a few hundred years ago, attributing the latter to the LIA. However, their LIA ages are very scattered and as such, do not allow the definition of a precise timing of the glacier advance. Glazirin (1993) reconstructed the ice-marginal positions of Abramov Glacier and assumed the end of the LIA moraine as 1850 (3630 m a.s.l.; Fig. 8), the year the glaciers in central Asia started a widespread retreat. Later, Solomina & Kamnyanskiy (1998), based on lichenometry, suggested an age of deposition for this moraine around the end of the 18th century. Our dating results allow us to define more precisely the age of this moraine formation as approximately 1750 CE.

Li *et al.* (2016) suggested two glacier advances in the Tien Shan during the LIA at 0.430±0.100 and 0.270±0.055 ka, with the former being the most extensive. Similar ages for the LIA advances in the Tien Shan were obtained by Zhang *et al.* (2016) and Koppes *et al.* (2008). These ages are also supported by proxy data analyses on speleothems (Cheng *et al.* 2020) and lichenometry (Solomina *et al.* 2004) suggesting wetter climatic conditions in eastern Tien Shan during this time (Solomina *et al.* 2004; Cheng *et al.* 2020). Recently, Leroy & Giralt (2021), based on pollen records, reconstructed palaeoclimatic conditions around the Issyk-Kul Lake for the past 5600 years and linked the cooler conditions, such as during the LIA, to more enhanced Westerlies. The obtained cosmogenic ^{10}Be ages for the LIA advance in our study area correspond well to the more recent glacier advance of around 270 a, suggested by Li *et al.* (2016), while traces of the older, more extensive glacier advance could have been destroyed by fluvial and slope processes.

Mean specific mass balance (<*b*>) reconstruction suggests a gradually more negative mass balance since

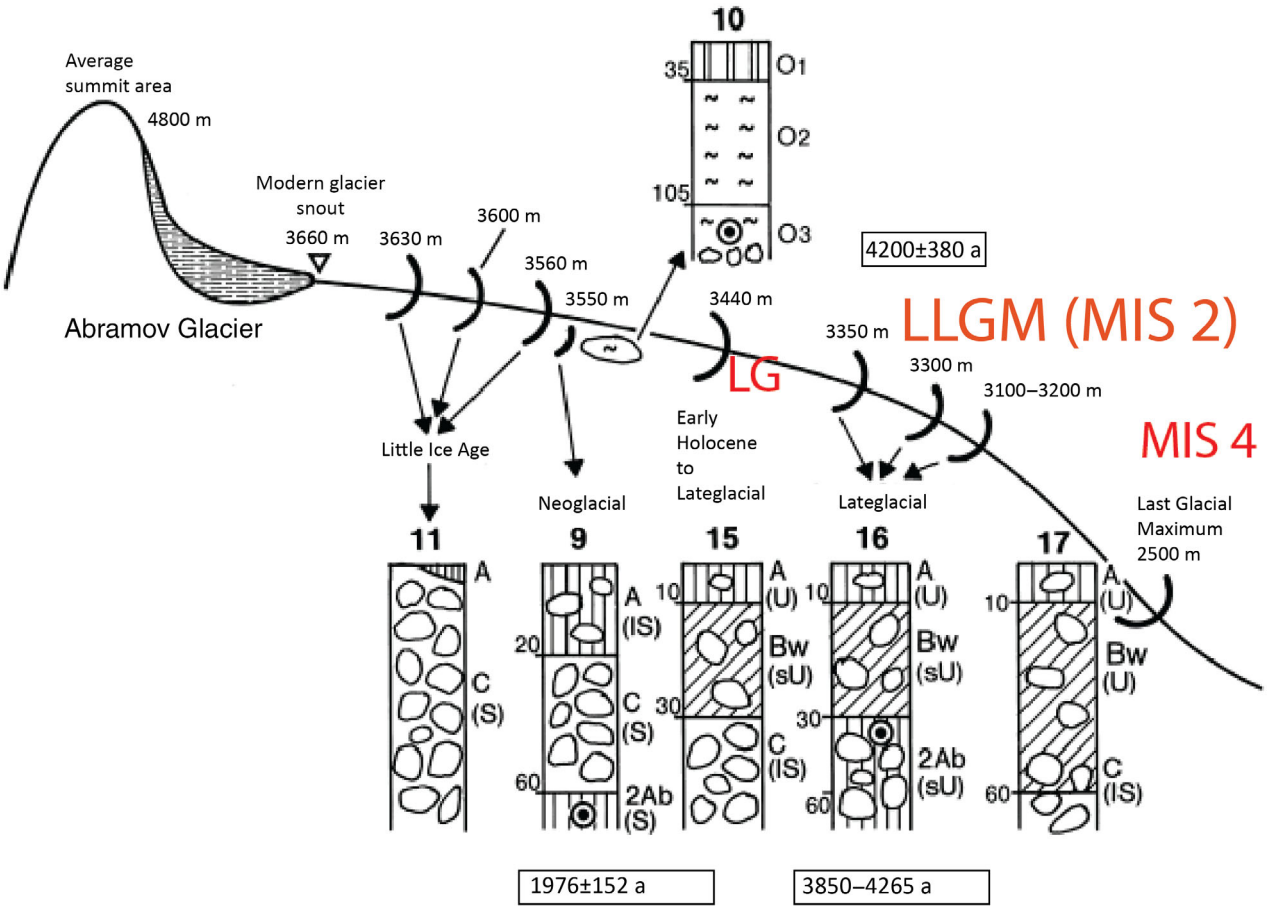

Fig. 8. Altitude of moraines in the Koksu valley and soil profiles, modified and reinterpreted after Zech *et al.* (2000). A = surface horizon; Ab = buried surface horizon; Bw = cambic horizon; C = parent material; O = peat; S = sand; IS = loamy sand; U = silt; sU = sandy silt. The radiocarbon ages were recalculated using the software Calib8.2 and the calibration curve IntCal20 (Reimer *et al.* 2020). The reinterpreted moraine ages are in red. LG = Lateglacial; LLGM = Local Last Glacial Maximum; MIS 4 = Marine Isotope Stage 4 glacial advance. The numbers above the borehole logs indicate the number of the borehole as described in Zech *et al.* (2000).

the LIA advance (Fig. 7). The mean specific mass balance decrease accelerated during the last quarter of the 20th century. Azisov *et al.* (2022) reconstructed the mean specific mass balance for the Golubin glacier in the Ala-Archa catchment, Kyrgyz Ala-Too range, in northern Tien Shan since 1850. Their results suggest a similar gradual decrease in mass balance until the 1970s and a more rapid decrease in the last quarter of the 20th century. Reconstructed mean annual specific mass balance for the time period from 1980 until 2016 (−0.29 m w.e. per year) roughly matches the mean observed annual mass balance for the same period (−0.36 m w.e. per year (WGMS 2021)). The mean geodetic annual mass balance calculated by Denzinger *et al.* (2021) for the time period of 1975–2015 is −0.38 m w.e. per year, lower than the mean annual specific mass balance calculated here, indicating that Abramov Glacier has been in climatic disequilibrium in recent decades.

Solomina (2000) and Solomina *et al.* (2004) estimated that during the LIA the ELAs were 60–70 m lower than present for the glaciers of the Pamir-Alay, while Zech *et al.* (2000) estimated that the ELA during the LIA was 50 m lower compared to the present. Our simulation with the AABR method suggests an ELA 70 m lower than present during the LIA. The GFM modelling results suggest an ELA depression of 80 m. Our results with both AABR and the GFM model support earlier ELA estimations. The modelling results show good agreement with GPR measurements. Maximum thickness for the present-day simulation (ELA at 4100 m a.s.l.; Fig. 6B) is 218 m, while the GPR measurements from 1986 (Kuzmichenok 1990) suggest a maximum Abramov Glacier thickness of 228 m.

Conclusions

Our results suggest that glaciation in the Pamir-Alay reached its maximum extent around the LLGM (MIS 2), 15.6±0.5 to 18.7±0.5 ka BP. Further cosmogenic exposure ages are necessary to confirm the glaciation extent during MIS 2 as well as for a more detailed

reconstruction of the glacier dynamics during the Holocene. However, for the Late Holocene, our dating results suggest a LIA glacier stage at 1750 CE, some 100 years earlier than previously suggested. During this stage, the ELA was 70 to 80 m lower than present. The reconstructed secular glacier mass balance suggests a gradual glacier retreat until the second half of the 20th century. From that time, the mass loss rate has steadily increased. The mean annual specific mass balance $<b>$ for the whole period since the LIA was around −0.32 m w.e. per year. For the time period since the LIA (1750 CE) until the start of the 20th century, the mean annual mass balance $<b>$ was close to equilibrium (−0.06 m w.e. per year) and mass loss has gradually accelerated since then. Our results also suggest that Abramov Glacier has been increasingly in disequilibrium with the climate over the past two decades. This is supported by repeated GPR measurements of the tongue area suggesting a dramatic decrease of glacier area and ice volume in the time period from 1986 to 2018.

Acknowledgements. – We thank the Federal Office of Meteorology and Climatology MeteoSwiss for financing the project Capacity Building and Twinning for Climate Observing Systems (CATCOS), contract no. 7F-08114.1, between the Swiss Agency for Development and Cooperation and MeteoSwiss; the project Cryospheric Climate Services for improved Adaptation (CICADA), contract no. 81049674; and the project Cryospheric Observation and Modelling for Improved Adaptation in central Asia (CROMO-ADAPT), contract no. 81072443, between the Swiss Agency for Development and Cooperation and the University of Fribourg. The SPI Flagship Initiative with the project PAMIR (grant number: SPI-FLAG-2021-001). The French national AMS facility ASTER (CEREGE) is supported by the INSU/CNRS, the French MESR, and the CEA institute. We thank Eric Pohl for support in processing the figures. We are also grateful to Andrejs Timuhins for his help with data analysis. The comments from one anonymous reviewer and from A. Ribolini improved the final manuscript. The authors declare that the research was conducted in the absence of any commercial or financial relationships that could be construed as a potential conflict of interest.

Author contributions. – TS conducted the fieldwork, glacier modelling studies and interpretation of the results. VR carried out the ^{10}Be sample preparation, dating and interpretation. IL led the GPR measurements and interpretation. GB carried out the Abramov Glacier surface reconstruction. EM substantially improved the glacier flow model and contributed to modelling. MH contributed to the interpretation of the results.

Data availability statement. – The data that support the findings of this study are available from the corresponding author upon reasonable request.

References

Abramowski, U., Bergau, A., Seebach, D., Zech, R., Glaser, B., Sosin, P., Kubik, P. V. & Zech, W. 2006: Pleistocene glaciations of Central Asia: results from 10Be surface exposure ages of erratic boulders from the Pamir (Tajikistan), and the Alay-Turkestan range (Kyrgyzstan). *Quaternary Science Reviews 25*, 9–10.

Arnold, M., Merchel, S., Bourlès, D. L., Braucher, R., Benedetti, L., Finkel, R. C., Aumaître, G., Gottdang, A. & Klein, M. 2010: The French accelerator mass spectrometry facility ASTER: improved performance and developments. *Nuclear Instruments and Methods in Physics Research, Section B: Beam Interactions with Materials and Atoms 268*, 11–12.

Azisov, E., Hoelzle, M., Vorogushyn, S., Saks, T., Usubaliev, R., Esenaman Uulu, M. & Barandun, M. 2022: Reconstructed centennial mass balance change for Golubin Glacier, Northern Tien Shan. *Atmosphere 13*, 954, https://doi.org/10.3390/atmos13060954.

Balco, G., Stone, J. O., Lifton, N. A. & Dunai, T. J. 2008: A complete and easily accessible means of calculating surface exposure ages or erosion rates from ^{10}Be and ^{26}Al measurements. *Quaternary Geochronology 3*, 174–195.

Barandun, M., Fiddes, J., Scherler, M., Mathys, T., Saks, T., Petrakov, D. & Hoelzle, M. 2020: The state and future of the cryosphere in Central Asia. *Water Security 11*, 100072, https://doi.org/10.1016/j.wasec.2020.100072.

Barandun, M., Huss, M., Sold, L., Farinotti, D., Azisov, E., Salzmann, N., Usubaliev, R., Merkushkin, A. & Hoelzle, M. 2015: Re-analysis of seasonal mass balance at Abramov glacier 1968–2014. *Journal of Glaciology 61*, 1103–1117.

Batbaatar, J., Gillespie, A. R., Koppes, M., Clark, D. H., Chadwick, O. A., Fink, D., Matmon, A. & Rupper, S. 2020: Glacier development in continental climate regions of central Asia. *In* Waitt, R. B., Thackray, G. D. & Gillespie, A. R. (eds.): *Untangling the Quaternary Period—A Legacy of Stephen C. Porter*, 123–154. *Geological Society of America Special Papers 548*.

Benn, D. I. & Hulton, N. R. 2010: An Excel™ spreadsheet program for reconstructing the surface profile of former mountain glaciers and ice caps. *Computers and Geosciences 36*, 605–610.

Blomdin, R., Stroeven, A. P., Harbor, J. M., Lifton, N. A., Heyman, J., Gribenski, N., Petrakov, D. A., Caffee, M. W., Ivanov, M. N., Hättestrand, C., Rogozhina, I. & Usubaliev, R. 2016: Evaluating the timing of former glacier expansions in the Tian Shan: a key step towards robust spatial correlations. *Quaternary Science Reviews 153*, 78–96.

Bondarev, L. G., Gobedzhishvili, R. G. & Solomina, O. N. 1997: Fluctuations of local glaciers in the southern ranges of the former USSR: 18,000-8000 BP. *Quaternary International 38-39*, 103–108.

Borchers, B., Marrero, S., Balco, G., Caffee, M., Goehring, B., Lifton, N., Nishiizumi, K., Phillips, F., Schaefer, J. & Stone, J. 2016: Geological calibration of spallation production rates in the CRONUS-Earth project. *Quaternary Geochronology 31*, 188–198.

Brædstrup, C. F., Egholm, D. L., Ugelvig, S. V. & Pedersen, V. K. 2016: Basal shear stress under alpine glaciers: insights from experiments using the iSOSIA and Elmer/Ice models. *Earth Surface Dynamics 4*, 159–174.

Braucher, R., Guillou, V., Bourlès, D. L., Arnold, M., Aumaître, G., Keddadouche, K. & Nottoli, E. 2015: Preparation of ASTER in-house ^{10}Be/^{9}Be standard solutions. *Nuclear Instruments and Methods in Physics Research, Section B: Beam Interactions with Materials and Atoms 361*, 335–340.

Cheng, H., Zhang, H., Spötl, C., Baker, J., Sinha, A., Li, H., Bartolomé, M., Moreno, A., Kathayat, G., Zhao, J., Dong, X., Li, Y., Ning, Y., Jia, X., Zong, B., Ait Brahim, Y., Pérez-Mejías, C., Cai, Y., Novello, V. F., Cruz, F. W., Severinghaus, J. P., An, Z. & Edwards, R. L. 2020: Timing and structure of the Younger Dryas event and its underlying climate dynamics. *Proceedings of the National Academy of Sciences of the United States of America 117*, 23408–23417.

Child, D., Elliott, G., Mifsud, C., Smith, A. M. & Fink, D. 2000: Sample processing for earth science studies at ANTARES. *Nuclear Instruments and Methods in Physics Research, Section B: Beam Interactions with Materials and Atoms 172*, 1–4.

Chmeleff, J., von Blanckenburg, F., Kossert, K. & Jakob, D. 2010: Determination of the ^{10}Be half-life by multicollector ICP-MS and liquid scintillation counting. *Nuclear Instruments and Methods in Physics Research, Section B: Beam Interactions with Materials and Atoms 268*, 192–199.

Cuffey, K. M. & Paterson, W. S. 2010: *The Physics of Glaciers*. 683 pp. Elsevier, Amsterdam.

Denzinger, F., Machguth, H., Barandun, M., Berthier, E., Girod, L., Kronenberg, M., Usubaliev, R. & Hoelzle, M. 2021: Geodetic mass

balance of Abramov Glacier from 1975 to 2015. *Journal of Glaciology 67*, 331–342.
Dowdeswell, J. A. 2004: Investigations of the form and flow of ice sheets and glaciers using radio-echo sounding. *Reports on Progress in Physics 67*, 1821–1861.
Evans, I. & Cox, N. 2005: Global variations of local asymmetry in glacier altitude: separation of north-south and east-west components. *Journal of Glaciology 51*, 469–482.
Farinotti, D., Huss, M., Fürst, J. J., Landmann, J., Machguth, H., Maussion, F. & Pandit, A. 2019: A consensus estimate for the ice thickness distribution of all glaciers on Earth. *Nature Geoscience 12*, 168–173.
Ficker, H. 1933: Die eiszeitliche Vergletscherung der nordwestlichen Pamirgebiete. Sitzungsberichte der Preussischen Akademie der Wissenschaften, Physikalisch-Mathematische Klasse, 61–86.
Fowler, A. C. & Larson, D. A. 1978: On the flow of polythermal glaciers: I. Model and preliminary analysis. *Proceedings of the Royal Society of London 363*, 217–242.
Gastaldello, M. A. 2022: *Analysing Mass Balance Gradient*. University of Fribourg, Fribourg.
Glazirin, G. 1993: *Regime of Abramov Glacier*. 228 pp. Hydrometeo Publishing, Leningrad.
Grin, E., Ehlers, T. A., Schaller, M., Sulaymonova, V., Ratschbacher, L. & Gloaguen, R. 2016: 10Be surface-exposure age dating of the Last Glacial Maximum in the northern Pamir (Tajikistan). *Quaternary Geochronology 34*, 47–57.
Haeberli, W. & Hoelzle, M. 1995: Application of inventory data for estimating characteristics of and regional climate-change effects on mountain glaciers: a pilot study with the European Alps. *Annals of Glaciology 21*, 206–212.
Herber, L. 1969: Separation of feldspar from quartz by flotation. *American Mineralogist 54*, 1212–1215.
Hoelzle, M., Azisov, E., Barandun, M., Huss, M., Farinotti, D., Gafurov, A., Hagg, W., Kenzhebaev, R., Kronenberg, M., Machguth, H., Merkushkin, A., Moldobekob, B., Petrov, M., Saks, T., Salzmann, N., Schöne, T., Tarasov, Y., Usubaliev, R., Vorogushyn, S., Yakovlev, A. & Zemp, M. 2017: Re-establishing glacier monitoring in Kyrgyzstan and Uzbekistan, Central Asia. *Geoscientific Instrumentation, Methods and Data Systems 6*, 397–418.
Hoelzle, M., Chinn, T., Stumm, D., Paul, F., Zemp, M. & Haeberli, W. 2007: The application of glacier inventory data for estimating past climate change effects on mountain glaciers: a comparison between the European Alps and the Southern Alps of New Zealand. *Global and Planetary Change 56*, 69–82.
Hoelzle, M., Haeberli, W., Dischl, M. & Peschke, W. 2003: Secular glacier mass balances derived from cumulative glacier length changes. *Global and Planetary Change 36*, 295–306.
Huss, M., Bauder, A., Linsbauer, A., Gabbi, J., Kappenberger, G., Steinegger, U. & Farinotti, D. 2021: More than a century of direct glaciermass-balance observations on Claridenfirn, Switzerland. *Journal of Glaciology 67*, 697–713.
Johannesson, T., Raymond, C. & Waddington, E. 1989: Time-scale for adjustment of glaciers to changes in mass balance. *Journal of Glaciology 35*, 355–369.
Klebelsberg, R. V. 1934: The glacial and glacial geological results of the Alai Pamir Expedition 1928. *Journal of Glaciology 21*, 205–212.
Kohl, C. P. & Nishiizumi, K. 1992: Chemical isolation of quartz for measurement of in-situ -produced cosmogenic nuclides. *Geochimica et Cosmochimica Acta 56*, 3583–3587.
Koppes, M., Gillespie, A. R., Burke, R. M., Thompson, S. C. & Stone, J. 2008: Late Quaternary glaciation in the Kyrgyz Tien Shan. *Quaternary Science Reviews 27*, 846–866.
Korschinek, G., Bergmaier, A., Faestermann, T., Gerstmann, U. C., Knie, K., Rugel, G., Wallner, A., Dillmann, I., Dollinger, G., Lierse von Gostomski, C. H., Kossert, K., Mait, K., Poutivtsev, M. & Remmert, A. 2010: A new value for the half-life of ^{10}Be by Heavy-Ion Elastic Recoil Detection and liquid scintillation counting. *Nuclear Instruments and Methods in Physics Research, Section B: Beam Interactions with Materials and Atoms 268*, 187–191.
Kronenberg, M., Machguth, H., Eichler, A., Schwikowski, M. & Hoelzle, M. 2021: Comparison of historical and recent accumulation rates on Abramov Glacier, Pamir Alay. *Journal of Glaciology 67*, 253–268.
Kronenberg, M., van Pelt, W., Machguth, H., Fiddes, J., Hoelzle, M. & Pertziger, F. 2022: Long-term firn and mass balance modelling for Abramov glacier in the data-scarce Pamir Alay. *The Cryosphere 16*, 5001–5022.
Kulnitsky, L. M. 2000: Matematicheskaya obrabotka dannykh georadiolokatsii i systema RADEXPRO (Mathematical processing of georadar data and RADEXPRO system). *Razvedka i Okhrana Nedr 21*, 6–11.
Kuzmichenok, V. 1990: Topographicheskaya s' emka rel'efa lozha lednikov radiolokacionnim metodom [Method of the glaciers surface and bedrock topography measurements by radioecho sounding]. *Geodesiya i Kartogrphiya 4*, 18–23.
Lal, D. 1991: Cosmic ray labeling of erosion surfaces: in situ nuclide production rates and erosion models. *Earth and Planetary Science Letters 104*, 424–439.
Leroy, S. A. & Giralt, S. R. 2021: Humid and cold periods in the last 5600 years in Arid Central Asia revealed by palynology of Picea schrenkiana from Issyk-Kul. *Holocene 31*, 380–391.
Li, Y., Li, Y., Harbor, J., Liu, G., Yi, C. & Caffee, M. W. 2016: Cosmogenic ^{10}Be constraints on Little Ice Age glacial advances in the eastern Tian Shan, China. *Quaternary Science Reviews 138*, 105–118.
Lifton, N., Beel, C., Hättestrand, C., Kassab, C., Rogozhina, I., Heermance, R., Oskin, M., Burbank, D., Blomdin, R., Gribenski, N., Caffee, M., Goehring, B. B., Heyman, J., Ivanov, M., Li, Y., Li, Y., Petrakov, D., Usubaliev, R., Codilean, T. A., Chen, Y., Harbor, J. & Stroeven, A. P. 2014: Constraints on the late Quaternary glacial history of the Inylchek and Sary-Dzaz valleys from in situ cosmogenic ^{10}Be and ^{26}Al, eastern Kyrgyz Tian Shan. *Quaternary Science Reviews 101*, 77–90.
Mandychev, A. N., Usubaliev, R. A. & Azisov, E. A. 2017: Changes of the Abramov Glacier (Alay Ridge) from 1850 to 2014. *Led i Sneg 57*, 326–333.
Mölg, N., Bolch, T., Rastner, P., Strozzi, T. & Paul, F. 2018: A consistent glacier inventory for Karakoram and Pamir derived from Landsat data: distribution of debris cover and mapping challenges. *Earth System Science Data 10*, 1807–1827.
Nichols, K. A. 2019: Isolation of quartz for cosmogenic in situ ^{14}C analysis. *Geochronology 1*, 43–52.
Nishiizumi, K. 1989: Cosmic ray production rates of ^{10}Be and ^{26}Al in quartz from glacially polished rocks. *Journal of Geophysical Research: Solid Earth 94*, 17907–17915.
Noeth, L. 1931: Glazialgeologische und morphologische Untersuchungen im Nordwest-Pamir. *Mitteilungen der Geographischen Gesellschaft in München 24*, 154–192.
O'Callaghan, J. F. & Mark, D. M. 1984: The extraction of drainage networks from digital elevation data. *Computer Vision, Graphics & Image Processing 28*, 323–344.
Ohmura, A. A. 2018: Climate on the equilibrium line altitudes of glaciers: theoretical background behind Ahlmann's P/T diagram. *Journal of Glaciology 64*, 489–505.
Osmaston, H. 2005: Estimates of glacier equilibrium line altitudes by the Area × Altitude, the Area × Altitude Balance Ratio and the Area × Altitude Balance Index methods and their validation. *Quaternary International 138-139*, 22–31.
Pellitero, R., Rea, B. R., Spagnolo, M., Bakke, J., Ivy-Ochs, S., Frew, C. R., Hughes, P., Ribolini, A., Likas, S. & Renssen, H. 2016: GlaRe, a GIS tool to reconstruct the 3D surface of palaeoglaciers. *Computers and Geosciences 94*, 77–85.
Reimer, P. J. and 41 others 2020: The IntCal20 northern hemisphere radiocarbon age calibration curve (0-55 cal kBP). *Radiocarbon 62*, 725–757.
RGI Consortium 2017: Randolph Glacier Inventory – a dataset of global glacier outlines: Version 6.0 GLIMS Technical Report RGI. *Global Land Ice Measurements from Space, Colorado, USA, Digital Media*, https://doi.org/10.7265/N5-RGI-60.
Rodriguez, E., Morris, C. & Belz, J. 2006: An assessment of the SRTM topographic products. *Photogrammetric Engineering and Remote Sensing 72*, 249–260.

Röhringer, I., Zech, R., Abramowski, U., Sosin, P., Aldahan, A., Kubik, P. W., Zöller, L. & Zech, W. 2012: The late Pleistocene glaciation in the Bogchigir Valleys (Pamir, Tajikistan) based on ^{10}Be surface exposure dating. *Quaternary Research 78*, 590–597.

Ryumin, A. 1972: Radiolokatsionnoye zondirovaniye lednika Abramova (Radio-echo sounding of Abramov glacier) (in Russian). *Trudi SANIGMI 65*, 73–83.

Seong, Y. B., Owen, L. A., Yi, C., Finkel, R. C. & Schoenbohm, L. 2009: Geomorphology of anomalously high glaciated mountains at the northwestern end of Tibet: Muztag Ata and Kongur Shan. *Geomorphology 103*, 227–250.

Sidorov, L. 1960: Early glaciation of the Pamirs. *Reports of the Academy of Science of the USSR Earth Science Sections 127*, 732–733 (in Russian).

Sidorov, L. 1979: *Nature of the Pamir during the Quaternary* (in Russian). 145 pp. Nauka Press, Moscow.

Solomina, O. N. 2000: Retreat of mountain glaciers of northern Eurasia since the Little Ice Age maximum. *Annals of Glaciology 31*, 26–30.

Solomina, A. N. & Kamnyanskiy, G. M. 1998: Fluctuations of four glaciers in Pamir-Alay, based on lichonometrical dating. *Materiali Glaciologicheskikh Izsledovaniy 84*, 158–164.

Solomina, O., Barry, R. & Bodnya, M. 2004: The retreat of Tien Shan glaciers (Kyrgyzstan) since the Little Ice Age estimated from aerial photographs, lichenometric and historical data. *Geografiska Annaler. Series A, Physical Geography 86*, 205–215.

Stone, J. O. 2000: Air pressure and cosmogenic isotope production. *Journal of Geophysical Research: Solid Earth 105*, 23753–23759.

Stübner, K., Bookhagen, B., Merchel, S., Lachner, J. & Gadoev, M. 2021: Unravelling the Pleistocene glacial history of the Pamir mountains, Central Asia. *Quaternary Science Reviews 257*, 106857, https://doi.org/10.1016/j.quascirev.2021.106857.

Suslov, V. F. 1972: On the question of the ancient glaciation of the Koksu river catchment. *Trudi SANIGMI* (in Russian). *65*, 96–101.

Taylor, J. R. 1997: *An Introduction to Error Analysis*. 327 pp. University Science Books, Sausalito.

Unterfinger, M. & Luck, M. A. 2023: Modeling glaciers on a digital elevation model based on mass balance and a modified D8 flow algorithm applied to ice. (v0.4.0). *Zenodo 2023*, https://doi.org/10.5281/zenodo.10269631.

Vasilenko, E. V. 2011: A compact lightweight multipurpose ground-penetrating radar for glaciological applications. *Journal of Glaciology 57*, 1113–1118.

Vasilenko, E. V., Gromyko, A. N., Konstantinova, T. N., Kuzmichenok, V. A., Macheret, Y., Moskalevsky, M. Y. & Shapo, K. I. 1988: Radiolokatsionnaya s'emka lednika Abramova nizkochastotnym lokatorom (Radio-echo sounding of Abramov glacier with low frequency radar). *Data of Glaciological Studies 64*, 174–182.

Weertman, J. 1964: The theory of glacier sliding. *Journal of Glaciology 5*, 287–303.

WGMS 2021: *Global Glacier Change Bulletin No. 4 (2018-2019)*. World Glacier Monitoring Service, Zurich.

Zech, R., Abramowski, U., Glaser, B., Sosin, P., Kubik, P. W. & Zech, W. 2005a: Late Quaternary glacial and climate history of the Pamir Mountains derived from cosmogenic ^{10}Be exposure ages. *Quaternary Research 64*, 212–220.

Zech, W., Glaser, B., Ni, A., Petrov, M. & Lemzin, I. 2000: Soils as indicators of the Pleistocene and Holocene landscape evolution in the Alay Range (Kyrgystan). *Quaternary International 65-66*, 161–169.

Zech, R., Glaser, B., Sosin, P., Kubik, P. W. & Zech, W. 2005b: Evidence for long-lasting landform surface instability on hummocky moraines in the Pamir Mountains (Tajikistan) from ^{10}Be surface exposure dating. *Earth and Planetary Science Letters 237*, 453–461.

Zech, R., Röhringer, I., Sosin, P., Kabgov, H., Merchel, S., Akhmadaliev, S. & Zech, W. 2013: Late Pleistocene glaciations in the Gissar Range, Tajikistan, based on 10Be surface exposure dating. *Palaeogeography, Palaeoclimatology, Palaeoecology 369*, 253–261.

Zemp, M., Huss, M., Thibert, E., Eckert, N., McNabb, R., Huber, J., Barandun, M., Machguth, H., Nussbaumer, U. S., Gärtner-Roer, I., Thomson, L., Paul, F., Maussion, F., Kutuzov, S. & Cogley, G. J. 2019: Global glacier mass changes and their contributions to sea-level rise from 1961 to 2016. *Nature 568*, 382–386.

Zhang, M., Chen, Y., Li, Y. & Liu, G. 2016: Late Quaternary glacial history of the Nalati Range, central Tian Shan, China, investigated using ^{10}Be surface exposure dating. *Journal of Quaternary Science 31*, 659–670.